Forbidden electron attachment in O_2

Hideo Sambe and David E. Ramaker

Department of Chemistry, George Washington University, Washington, D.C. 20052

(Received 6 October 1988)

The electron-stimulated O^- desorption yield from condensed O_2 exhibits three peaks around 7, 8.5, and 13 eV, while that from O_2 gas shows only the 7-eV peak. The 7-eV peak is known to arise from the $O_2^-(1\pi_u^{-1}1\pi_g^2)^2\Pi_u$ compound state. In this paper the 8.5- and 13-eV peaks are shown to arise from the $O_2^-(3\sigma_g^{-1}1\pi_g^2)^2\Sigma_g^+$ and $O_2^-(2\sigma_u^{-1}1\pi_g^2)^2\Sigma_u^+$ compound states, respectively. The absence of the 8.5- and 13-eV peaks in the gas-phase spectrum presents the first experimental evidence for a forbidden electron attachment, which is due to the σ^- selection rule [H. Sambe and D. E. Ramaker, Chem. Phys. Lett. **139**, 386 (1987)].

I. INTRODUCTION

In collisions of electrons with molecules, an electron may attach to a molecule, forming a temporary negative ion or a negative compound state. The production of this compound state is governed by certain selection rules. The selection rules are the following: (1) An allowed compound state must have either $|S-\frac{1}{2}|$ or $|S+\frac{1}{2}|$ total spin, when the target molecule has total spin S; (2) it should have an electronic configuration that differs by less than three-electron excitations with respect to the initial state (i.e., the target molecule plus an incident electron), and (3) it must not have Σ^- (Σ^+) symmetry, if the target molecule is linear and has Σ^+ (Σ^-) symmetry. When any of the three rules is not satisfied, we use the term "forbidden electron attachment" by analogy with forbidden optical transitions. The last selection rule (3), which is similar to earlier selection rules by Cartwright *et al.*[1] and Dunn[2] but not identical, has been presented just recently and called the σ^- selection rule.[3]

Compound states which are forbidden in the gas phase may not be forbidden in the solid phase because of distortion of the local symmetry. Although the selection rules involving spin symmetry and number of electron excitations may persist in the solid phase, the rule involving cylindrical symmetry of linear molecules (or the σ^- selection rule) may relax in the solid phase. In fact, this breakdown of cylindrical symmetry has been clearly ob-

served in optical transitions.[4] In this paper, we study O_2 molecular systems in the gas and solid phases and identify, for the first time, the compound states which are forbidden by the σ^- selection rule.

In Sec. II, we analyze some experimental data previously published in the literature. Our findings are summarized in Table I. In Sec. III, various properties of the lower-lying O_2^- compound states are predicted utilizing empirical methods. These properties are summarized in Table II. In Sec. IV, we identify the forbidden compound states by comparing experimental (Table I) and theoretical (Table II) results. Finally in Sec. V, we review previous work.

II. EXPERIMENTAL RESULTS

A. Energy dependence of the O^- yields

Figure 1 shows electron-stimulated O^- desorption yields from various samples (O_2/W, O_2/Pt, and O_2 gas) as a function of the incident electron energy. These O^- yield curves are reproduced from figures previously published in the literature.[5-8] The relative magnitudes of these curves do not represent the actual relative O^- yields. For example, the O^- yield from O_2 gas (dotted curve[5]) is arbitrarily normalized to the peak of the O_2/Pt curve for comparison. For the O_2/W data,[6] a polycrystalline W ribbon was dosed with 10 L (Langmuirs, 1

TABLE I. Summary of experimental findings on the 7-, 8.5-, and 13-eV O_2^- compound states.

State	Vertical energy (eV)[a]	O^- yield from O_2 gas	O^- yield from O_2 solid	FWHM (eV)[b]	Dissociation limit
7 eV	6.7	Large	Large	2.0 ± 0.2	1[c]
8.5 eV	8–9	Negligible	Large	2.2 ± 0.3	1
13 eV	13	Negligible	Large	2.1 ± 0.4	2

[a]From the O_2 ground state to peak positions in the O^- yield curves.
[b]Widths observed in the ion-yield curves.
[c]1 and 2 denote the lowest and the second lowest $O+O^-$ dissociation limits.

TABLE II. Properties of the lower-lying O_2^- valence states.

Electronic configuration	Symmetry	Vertical energy (eV)	Electron attachment	$\Delta W(R_e)$ (eV)	ΔR_{ec} (Å)	Width (eV)	Dissociation limit
$1\pi_g$	$^2\Pi_g(I)$	0.21	$A(1)$	0.31	0.04	1.2	1
$1\pi_u^{-1}1\pi_g^2$	$^2\Pi_u(I)$	7.8±0.2	$A(2)$	1.8	0.18	3.0	1
$3\sigma_g^{-1}1\pi_g^2$	$^2\Sigma_g^+(I)$	8.1±0.9	F	(0.4)	(0.04)	(2.4)	1
$2\sigma_u^{-1}1\pi_g^2$	$^2\Sigma_u^+(II)$	14.3±0.9	F	(0.1)	(0.01)	(2.2)	2
$3\sigma_u$	$^4\Sigma_u^-(I)$	9.5±0.3	$A(1)$	9.6	0.39	4.3	1
	$^2\Delta_u(I)$	10.7±0.5	$A(2)$	9.8	0.39	(4.4)	1
	$^2\Sigma_u^+(I)$	11.5±0.5	F	10.0	0.40	(4.4)	1
	$^2\Sigma_u^-(I)$	11.9±0.4	$A(1)$	12.0	0.59	4.5	1
$1\pi_u^{-1}1\pi_g 3\sigma_u$	$^4\Sigma_g^+$		F				1
	$^4\Sigma_g^-$		$A(2)$				1
	$^4\Delta_g$	(17.5±1.0)[a]	$A(2)$	(10.0)	(0.4)	(6.3)	1
	$^2\Sigma_g^+(II)$		F				2
	$^2\Sigma_g^-$		$A(2)$				1
	$^2\Delta_g$		$A(2)$				1,2
$3\sigma_g^{-1}1\pi_g 3\sigma_u$	$^4\Pi_u$	(18.1±1.0)[a]	$A(2)$	(10.0)	(0.4)	(5.7)	1
	$^2\Pi_u$		$A(2)$				1,2

[a]Configuration center.
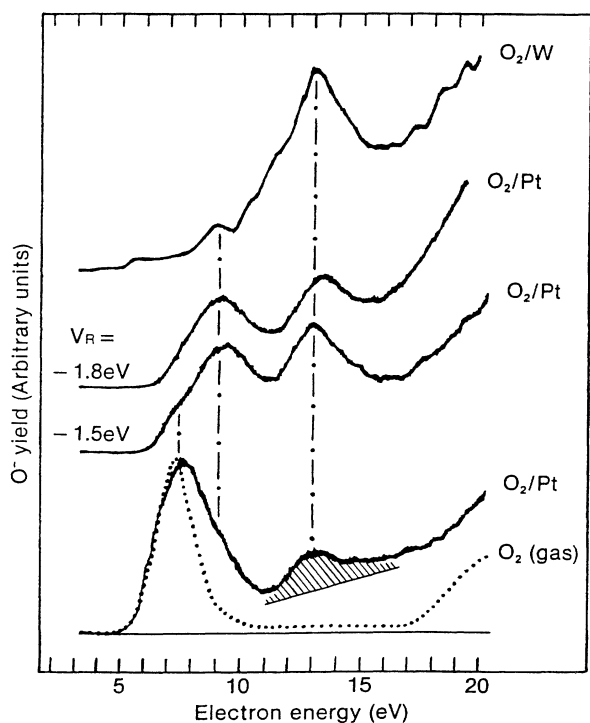
FIG. 1. Previously reported electron stimulated O^- desorption yields from O_2/W (Ref. 6), O_2/Pt (Refs. 7 and 8), and O_2 gas (Ref. 5) are plotted as a function of the incident electron energy. V_R denotes the retarding potential applied to the outgoing O^- ions. The shaded area shows our estimated contribution due to the direct process. The vertical dot-dashed lines indicate the probable peak positions of the involved O_2^- compound states.

$L = 10^{-6}$ Torr sec) of O_2 at room temperature. All three O_2/Pt samples[7,8] were prepared by condensing O_2 gas on a polycrystalline Pt ribbon at 20 K with a constant O_2 dosage. The estimated O_2 film thickness is 3 monolayers (ML) for all three Pt samples. Two of the three curves for O_2/Pt are measured with retarding potentials ($V_R = -1.5$ and -1.8 eV) against the outgoing O^- ions. The $V_R = -1.8$ eV retarding potential, for example, discriminates O^- ions whose kinetic energies outside the condensed film are less than 1.8 eV. The shaded area shows our estimated contribution due to the direct process, which we shall discuss later. Figure 2 shows the OH^- yield from $C_6H_{14}(1$ ML$)/O_2(3$ ML$)/Pt$ and the $O_2 \cdot O^-$ and O_2^- yields from the $(O_2)_n$ cluster. These curves are reproduced from Refs. 8 and 9, respectively. The O^- yield from O_2 gas (dotted curve) is shown again for comparison.

The O^- ions from O_2 are generated by the reaction

$$e^- + O_2 \to O_2^- \to O + O^- , \tag{1}$$
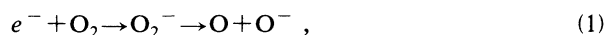
so that maxima in the O^- yield curve reflect the positions of O_2^- compound states. The OH^- yields from C_nH_{2n+2}/O_2 also reflect the positions of O_2^- compound states, because the OH^- ions are generated by two steps; namely, reaction (1) followed by

$$O^- + C_nH_{2n+2} \to OH^- + C_nH_{2n+1} , \tag{2}$$
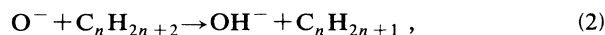
according to Sanche and Parenteau.[8] Similarly, $O_2 \cdot O^-$ and O_2^- ions from O_2 clusters are generated via the initial step

$$e^- + (O_2)_n \to (O_2)_{n-1} \cdot O_2^- . \tag{3}$$
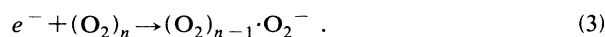
Therefore, the $O_2 \cdot O^-$ and O_2^- yield curves also reflect the positions of O_2^- compound states.

Figures 1 and 2 exhibit three peaks around 7, 8.5, and 13 eV as indicated in the two figures. The 8.5-eV peak in $(O_2)_n$ curves (Fig. 2) has been interpreted as a shift of the 7-eV state due to the polarization of the $(O_2)_n$ cluster.[9] Also the 8.5-eV peak in O_2/Pt curves (Fig. 1) was not ascribed to another compound state.[7] In this work, we attribute the 8.5-eV peak to another O_2^- compound state, based on the following four reasons: (1) Any polarization of the $(O_2)_n$ clusters should shift the 7-eV peak to lower energy, contrary to that observed. (2) The peak position of the 8.5-eV feature does not shift to higher energy, when the retarding potential is increased from -1.5 to -1.8 eV. In addition, there is an indication of a shoulder around 7 eV in the O_2/Pt ($V_R = -1.5$ eV) curve, suggesting that the 7-eV peak has not been shifted. (3) All ion-yield curves measured without retarding potentials, except the O^- yield curve from gaseous O_2, indicate the presence of the 8.5-eV feature. In fact, the 8.5-eV feature dominates in the O_2^--$(O_2)_n$ curve of Fig. 2. (4) Theory predicts three O_2^- compound states in the energy range from 7 to 15 eV, which can dissociate into an $O+O^-$ limit. To sum up, the 7-, 8.5-, and 13-eV features we believe to arise from three different O_2^- compound states.

As seen in Figs. 1 and 2, the relative intensities of the three features depend strongly on the structure of the sample (such as the O_2 layer thickness, substrate, and cluster size), the detected ions (O^-, O_2^-, $O_2 \cdot O^-$, or OH^-), and the detection angle of the ions. However, to establish the nature of the forbidden electron attachment, analysis of these intensities is not essential. The only fact which is used in this work is that both the 8.5- and 13-eV features are absent (or negligible relative to the 7-eV feature) in the O^- yield curve of gaseous O_2 (see Figs. 1 and 2).

B. O^- kinetic-energy distributions

Figure 3 shows the kinetic-energy distributions of the O^- ions from O_2(3 ML)/Pt measured at various incident electron energies ($E_i = 5.7$, 7.7, 12, and 13 eV). These data were obtained by Azria et al.[7] with an electron-energy resolution of 0.3 eV and an ion-energy resolution of 0.5 eV. The relative O^- kinetic energy (E_{rel}) (the absolute scale of the O^- kinetic energy was not determined) is measured with respect to the peak energy of the $E_i = 5.7$ eV curve. The three symbols with horizontal bars (closed and open circles and open triangle) indicate three different contributions, which will be described later. The horizontal bar with a symbol indicates the possible range of the peak position for each contribution. In Fig. 4, these peak-position ranges are plotted as a function of

FIG. 2. Previously reported electron stimulated negative ion (O^-, $O_2 \cdot O^-$, O_2^-, or OH^-) desorption yields from O_2 gas (Ref. 5), $(O_2)_n$ clusters (Ref. 9), or C_6H_{14}/O_2/Pt (Ref. 8). The negative ion yields are plotted as a function of the incident electron energy. The vertical dot-dashed lines indicate the probable peak positions of the involved O_2^- compound states.
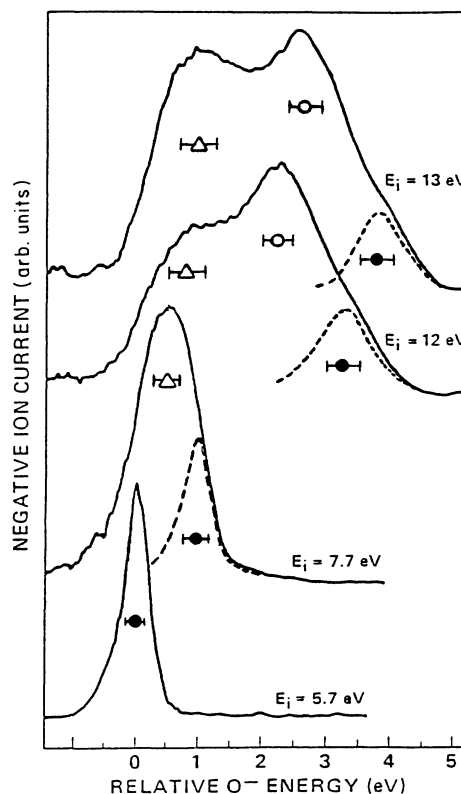
FIG. 3. Kinetic-energy distributions of the O^- ions from O_2(3 ML)/Pt (Ref. 7), which are measured at various incident electron energies, $E_i = 5.7$, 7.7, 12, and 13 eV. The ion energy is referred to the maximum in the distribution with $E_i = 5.7$ eV. Symbols (closed and open circles and open triangles) indicate three different contributions. The horizontal bar indicates the possible range of peak position for each contribution.
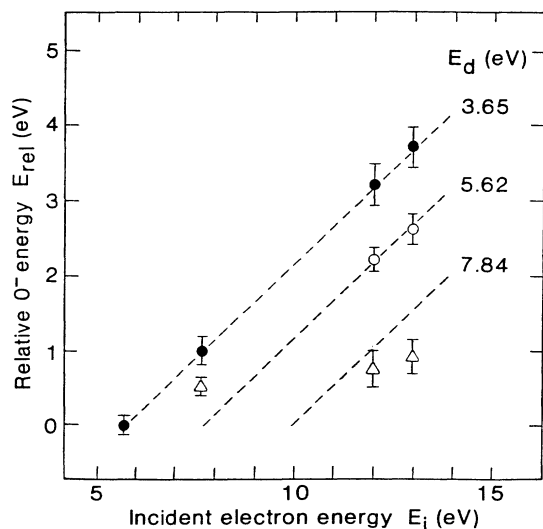
FIG. 4. The peak positions of the three contributions shown in Fig. 3 are plotted as a function of the incident electron energy E_i. The broken straight lines indicate E_{rel} given by Eq. (4). The E_d values denote the possible $O + O^-$ dissociation limits.

the incident electron energy E_i. The broken straight lines are given by the equation

$$E_{rel} = (E_i - E_d)/2 - 1.03 \text{ (eV)} , \tag{4}$$

where E_d is the relevant $O + O^-$ dissociation limit measured from the O_2 ground state ($v = 0$). The $E_d = 3.65$, 5.62, and 7.84 eV correspond to the lowest three dissociation limits, $O(^3P) + O^-(^2P)$, $O(^1D) + O^-(^2P)$, and $O(^1S) + O^-(^2P)$, respectively. The O^- kinetic energy (E_{abs}) from O_2 gas is given by

$$E_{abs} = (E_i - E_d)/2 , \tag{5}$$

where E_i and E_d have the same meanings of those of Eq. (4). The constant shift (1.03 eV) of E_{rel} with respect to E_{abs} arises from the artificial choice of the zero of energy for E_{rel} (i.e., $E_{rel} = 0$ for $E_i = 5.7$ eV and $E_d = 3.65$ eV).

As seen in Fig. 4, the features denoted by closed circles fit well on the straight line with $E_d = 3.65$ eV, indicating that they arise from the process

$$e^- + O_2(^3\Sigma_g^-) \rightarrow O_2^- \rightarrow O(^3P) + O^-(^2P) . \tag{6}$$
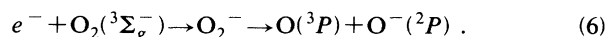
Similarly, the features with open circles fit well on the line with $E_d = 5.62$ eV, indicating that they arise from the process,

$$e^- + O_2(^3\Sigma_g^-) \rightarrow O_2^- \rightarrow O(^1D) + O^-(^2P) . \tag{7}$$
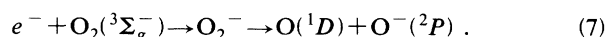
On the other hand, the features with open triangles do not fit on any of the lines. These features have been previously ascribed to the multiple scattering process,[7] that is,

$$e^- + O_2(^3\Sigma_g^-) \rightarrow O_2^* + e^{-'} \tag{8}$$

followed by

$$e^{-'} + O_2(^3\Sigma_g^-) \rightarrow O_2^- \rightarrow O(^3P) + O^-(^2P) . \tag{9}$$
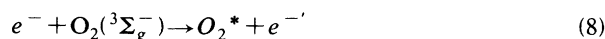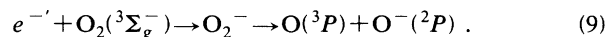
The above analysis supports this interpretation. A good fit to theory for the closed and open circles suggests that no significant amount of momentum is transferred to the O_2 lattice when the O^- desorbs from the surface. A similar conclusion was reached in the study of Cl^- desorption from condensed Cl_2.[10]

The O^- kinetic-energy distributions (Fig. 3) give information on the dissociation limits of the three O_2^- compound states. The curves at $E_i = 12$ and 13 eV show that the 13-eV compound state dissociates into the lowest two limits and the probability for dissociation into the second lowest limit is larger than that into the first. The $E_i = 7.7$ eV curve shows that the 7-eV compound state dissociates only into the lowest limit. The dissociation limits of the 8.5-eV compound state cannot be obtained directly from Fig. 3; however, it can be deduced by the following argument. The 7-eV compound state yields predominantly 1.7-eV [$= (7.0 - 3.65)/2$] O^- ions, provided that the momentum transfer to the O_2 lattice is negligible. The retarding potential $V_R = -1.8$ eV is strong enough to discriminate such low-energy ions, and indeed the 7-eV peak disappears in the $V_R = -1.8$ eV curve (see Fig. 1). Similarly, if the 8.5-eV compound state predominantly dissociates into the second lowest limit, the dominant O^- kinetic energy would be 1.5 eV [$= (8.5 - 5.62)/2$]. The retarding potential $V_R = -1.8$ eV should discriminate such low-energy O^- ions. The presence of the 8.5-eV peak in the $V_R = -1.8$ eV curve (Fig. 1), therefore, indicates that the 8.5-eV compound state predominantly dissociates into the lowest limit.

C. Widths

The widths of the 8.5- and 13-eV features can be estimated from the curves in Figs. 1 and 2. From the O_2/Pt ($V_R = -1.5$ and -1.8 eV) curves in Fig. 1, we estimate the full width at half-maximum (FWHM) for the 8.5- and 13-eV features to be 2.3 ± 0.4 and 2.1 ± 0.4 eV, respectively. In these estimates, the energy spread of the electron beam (0.3 eV) has been taken into account. From the 8.5-eV feature in the $O_2^-/(O_2)_n$ curve and the 13-eV feature in the $OH^-/C_6H_{14}/O_2$ curve, we estimate their FWHM to be 2.2 ± 0.3 and 2.3 ± 0.4 eV, respectively. The energy spreads of the electron beams in these experiments are 0.5 eV (Ref. 9) and 0.3 eV (Ref. 8), respectively. The two estimates (i.e., 2.3 and 2.2 eV for the 8.5-eV feature and 2.1 and 2.3 eV for the 13-eV feature) agree reasonably well.

We can estimate the contribution of a compound state to the O^- yield curve utilizing its FWHM. The shaded area in Fig. 1 shows such a contribution estimated with a FWHM equal to 2.1 eV and the electron-beam spread equal to 0.3 eV for the 13-eV feature. Figure 1 indicates a slowly varying background under the 13-eV feature. This background is due to multiple-electron scattering and is expected to vary slowly. We have already seen the presence of multiple-electron scattering in the O^- kinetic-energy distribution (Fig. 3), namely the contributions marked with open triangles. The multiple-electron

scattering in Fig. 3 is about 50% at 13 eV, which agrees with the background contribution (about 50%) at 13 eV in Fig. 1. This agreement supports the FWHM equal to 2.1 eV estimate for the width of the 13-eV compound state.

In conclusion, we estimate the widths of the 8.5- and 13-eV features to be 2.2±0.3 and 2.1±0.4 eV, respectively. The width of the 7-eV feature, which is observed in the O^- yield curve of O_2 gas, is 2.0±0.2 eV (Refs. 5 and 11).

D. Summary

Table I summarizes the observed characteristics of the 7-, 8.5-, and 13-eV compound states. The vertical energies in the table are measured from the O_2 ground state ($v=0$) to the peaks observed in the ion-yield curves. The FWHM's are the widths observed in the ion-yield curves. The "1" and "2" in the "dissociation limit" column stand for the lowest and the second lowest $O+O^-$ dissociation limits. In Sec. IV, we shall identify these compound states using their characteristics listed here.

III. THEORETICAL ANALYSES

Table II summarizes the predicted properties of the lower-lying O_2^- valence states. We explain each property in the following subsections.

A. Vertical energies

The O_2^- valence states are identified by their electronic configurations (EC) and state symmetries. The vertical energies from the O_2 ground state are estimated with semi-empirical methods, which are described in Appendix A. The EC's listed in Table II are the lowest 7, and the next lowest EC is located around 24 eV, which is too high for the 8.5- and 13-eV features. We have excluded O_2^- Rydberg states, that is, the $v^{-1}Ryd^2$ states, from our considerations for the 8.5- and 13-eV compound states, because Rydberg states are not observed in the condensed O_2 (Ref. 12) and probably cannot exist in the solid phase.

B. Electron attachment

According to the selection rules described in Sec. I, we can classify electron attachments into three categories: allowed with one-electron excitation [$A(1)$], allowed with two-electron excitations [$A(2)$], and forbidden (F). The attachment probability of $A(1)$ excitations is generally much higher than that of $A(2)$. The classified electron attachments from the O_2 ground state ($^3\Sigma_g^-$) are listed in Table II. Although the formation of the $^2\Delta_u(3\sigma_u)$ state appears to be $A(1)$, it is not $A(1)$ but $A(2)$ because the $^2\Delta_u(3\sigma_u)$ state arises from the $1\pi_g^2(^1\Delta_g)3\sigma_u$ configuration but the initial state has the $1\pi_g^2(^3\Sigma_g^-)\epsilon\delta_u$ configuration. Here, $\epsilon\delta_u$ represents an incoming electron orbital of kinetic energy ϵ and symmetry δ_u. All forbidden attachments in the table are due to the σ^- selection rule.[3] These $\Sigma^- \nleftrightarrow \Sigma^+$ forbidden attachments are expected to relax in the solid phase; the analogous $\Sigma^- \nleftrightarrow \Sigma^+$ forbidden photoabsorption processes are indeed observed in solid O_2.[4]

C. Electron detachment

Figure 5 illustrates a dissociative attachment process accompanied with autodetachment or autoionization, also called electron detachment. The O_2^- state, which is formed by electron impact of energy E, autoionizes into an O_2 state, when $W^-(R) > W(R)$ or $R_E < R < R_C$. Here, $W^-(R)$ and $W(R)$ are the potential-energy curves of the O_2^- and O_2 states, R_E is the turning point of the $W^-(R)$ at the energy E, and R_C is the crossing point of the two potential curves (see Fig. 5). In order to dissociate into an $O+O^-$ limit, the O_2^- state must survive against the above-mentioned autoionization. According to Bardsley et $al.$,[13] the dissociative attachment cross section $\sigma_{DA}(E)$ for the above process is given approximately by

$$\sigma_{DA}(E) = \sigma_{AT}(E)\exp\left[-\int_{R_E}^{R_C} dR\ \Gamma(R)/\hbar V(R)\right], \quad (10)$$

where $\sigma_{AT}(E)$ is the cross section for formation of the O_2^- state, $\Gamma(R)$ is the width of the O_2^- state with respect to the autoionization, and $V(R)$ is the relative velocity of the nuclei. The exponential factor in Eq. (10) represents the probability that the O_2^- state survives against the autoionization.

$\Gamma(R)$ for one-electron processes, such as

$$O_2^-(1\pi_u^{-1}1\pi_g^2)^2\Pi_u \rightarrow O_2(1\pi_u^{-1}1\pi_g)^3\Sigma_u^+ + e^-, \quad (11)$$
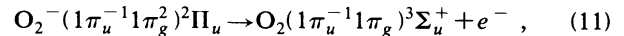
is governed by the kinetic energy of the outgoing electron [$\Delta W(R) = W^-(R) - W(R)$] and the asymptotic angular momentum l of the outgoing electron through the centrifugal barrier. For small ΔW, Γ is proportional to
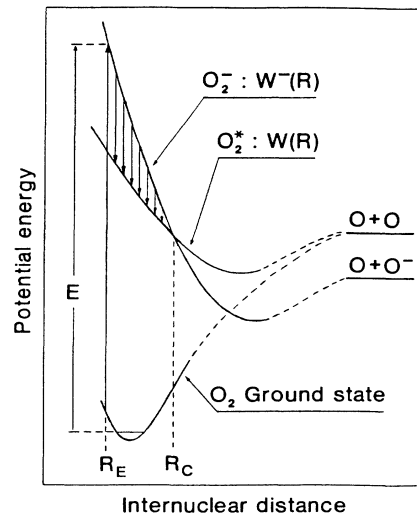
FIG. 5. Schematic potential-energy curves illustrating a dissociative attachment process accompanied with autodetachment. E is the energy of the incident electron. R_E is the turning point of potential curve $W^-(R)$ at the energy E, and R_C is the crossing point of the two potential curves, $W^-(R)$ and $W(R)$.

$$\Gamma \propto \Delta W^{l+1/2} \ , \tag{12}$$

for a one-electron process, and, in general, Γ increases monotonously with ΔW.[14] For two-electron processes, on the other hand, Γ is a slowly varying function of ΔW and is orders of magnitude smaller than that for one-electron processes, except for the $\Delta W \ll 1$ case. Since the survival factor depends exponentially on Γ, the survival factor for one-electron processes is several orders of magnitude smaller than that for two-electron processes except again for the $\Delta W \ll 1$ case.

The magnitude for autoionization via one-electron processes can be characterized by a pair of parameters, $\Delta W(R_e)$ and ΔR_{ec} $(=R_C - R_e)$, where R_e is the equilibrium internuclear distance for the O_2 ground state. Both parameters are referred to R_e because the initial O_2^- state is formed with the highest probability at $R = R_e$ according to the Franck-Condon principle. The larger the $\Delta W(R_e)$ and ΔR_{ec} parameters, the smaller the survival factor. Because of this property, these parameters play an important role in analyzing data. The $\Delta W(R_e)$ and ΔR_{ec} parameters are listed in Table II.

D. Franck-Condon widths

The width of the repulsive O_2^- compound state is predominantly governed by the Franck-Condon overlap integral between the $v = 0$ vibrational wave function of the O_2 ground state $\psi_0(R)$ and the vibrational wave function of the repulsive O_2^- compound state. In the reflection approximation,[15,16] the repulsive wave function can be replaced by a δ function which differs from zero only at the classical turning point. The results obtained with this replacement deviate only slightly from those obtained with accurate wave functions.[17] With this approximation, the Franck-Condon width (W_{FC}) of the repulsive O_2^- compound states can be given as

$$W_{FC} = \Delta R \, (v = 0) |dW^-(R)/dR|_{R=R_e} \ , \tag{13}$$

where $\Delta R \, (v = 0)$ is the FWHM of $\psi_0(R)^2$, because $W^-(R)$ of a repulsive state is nearly linear over the Franck-Condon region.

The W_{FC}'s in Table II are estimated from theoretical calculations in the literature, except for the W_{FC} of the $^2\Pi_u(1\pi_u^{-1}1\pi_g^2)$ state. The W_{FC} of this state is calculated from the experimental slope determined by O'Malley.[18] The slopes [i.e., $dW^-(R)/dR$ at $R = R_e$] for the $^2\Pi_g(1\pi_g)$, $^4\Sigma_u^-(3\sigma_u)$, and $^2\Sigma_u^-(3\sigma_u)$ states are calculated from the multiconfiguration self-consistent field (MCSCF) results[19] by quadratic curve fittings. The data in parentheses are estimated by assuming empirical relations such as

$$S(3\sigma_g^{-1}1\pi_g^2) - S(1\pi_u^{-1}1\pi_g^2) \approx S(3\sigma_g^{-1}1\pi_g)$$
$$- S(1\pi_u^{-1}1\pi_g) \ , \tag{14}$$

where S is the slope. The error ranges for the W_{FC}'s (2.4 and 2.2 eV) of the $^2\Sigma_g^+(3\sigma_g^{-1}1\pi_g^2)$ and $^2\Sigma_u^+(2\sigma_u^{-1}1\pi_g^2)$ states may be around ± 0.4 eV.

E. Dissociation limit

The dissociation limits of the lower-lying O_2^- valence states can be determined by the noncrossing rule. The molecular states resulting from the two lowest dissociation limits of $O + O^-$, known from Wigner-Witmer rules,[20] are listed in Table III. According to the noncrossing rule, these molecular states must be connected to the O_2^- valence states with the same symmetry without crossing each other. This implies, for example, that the lowest $^2\Sigma_u^+$ valence state must be connected to the lowest limit and the second lowest $^2\Sigma_u^+$ valence state to the second lowest limit. Another example, both the lowest

TABLE III. Dissociation limits of the O_2^- valence states which have the lower energies in the Franck-Condon region. Molecular states belonging to the dissociation are given in square brackets.

Dissociation limit	Symmetry	Electronic configuration	Vertical energy (eV)
$O^-(^2P_u) + O(^3P_g)$	$^2\Pi_g(I)$	$1\pi_g$	0.2
$[^2\Sigma_u^+, ^2\Sigma_g^+,$	$^2\Pi_u(I)$	$1\pi_u^{-1}1\pi_g^2$	7.8
$^4\Sigma_u^+, ^4\Sigma_g^+,$	$^2\Sigma_g^+(I)$	$3\sigma_g^{-1}1\pi_g^2$	8.1
$^2\Sigma_u^-(2), ^2\Sigma_g^-(2),$	$^4\Sigma_u^-(I)$	$3\sigma_u$	9.5
$^4\Sigma_u^-(2), ^4\Sigma_g^-(2),$	$^2\Delta_u(I)$	$3\sigma_u$	10.7
$^2\Pi_u(2), ^2\Pi_g(2),$	$^2\Sigma_u^+(I)$	$3\sigma_u$	11.5
$^4\Pi_u(2), ^4\Pi_g(2),$	$^2\Sigma_u^-(I)$	$3\sigma_u$	11.9
$^2\Delta_u, ^2\Delta_g,$			
$^4\Delta_u, ^4\Delta_g]$			
$O^-(^2P_u) + O(^1D_g)$	$^2\Sigma_u^+(II)$	$2\sigma_u^{-1}1\pi_g^2$	14.3
$[^2\Sigma_u^+(2), ^2\Sigma_q^+(2),$	$^2\Sigma_g^+(II)$	$1\pi_u^{-1}1\pi_g 3\sigma_u$	17
$^2\Sigma_u^-, ^2\Sigma_g^-,$			
$^2\Phi_u, ^2\Phi_g,$			
$^2\Pi_u(3), ^2\Pi_g(3),$			
$^2\Delta_u(2), ^2\Delta_g(2)]$			
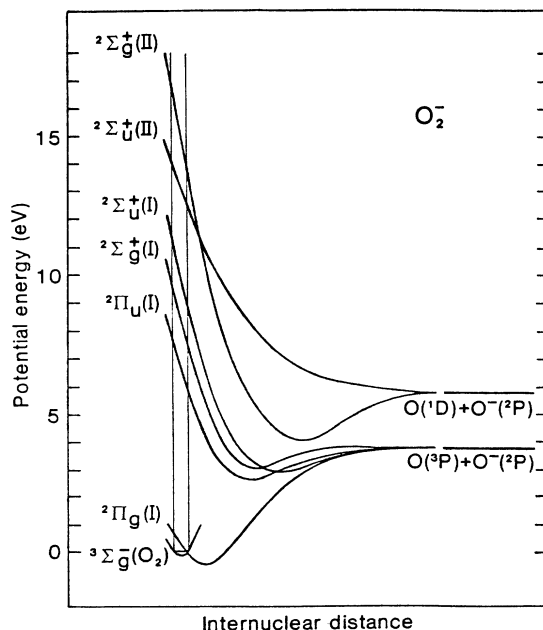
FIG. 6. Semiquantitative potential-energy curves, which are based on the data in Table II and the theoretical calculations of Refs. 21 and 22.

two $^2\Pi_g$ valence states must be connected to the lowest $^2\Phi_u$ valence state to the second lowest limit. Dissociation limits determined as above are listed in Table II, where 1 and 2 denote the lowest and the second lowest dissociation limits, respectively.

Figure 6 shows schematically the potential curves for some of the O_2^- valence states. These curves are drawn based on the data in Table II (such as the vertical energy, W_{FC}, and dissociation limit) and two theoretical calculations,[21,22] which were carried out only for large internuclear distances $(R > 1.6$ Å). The apparent avoided curve crossing between the two $^2\Sigma_g^+$ curves arises from the fact that the lowest $^2\Sigma_g^+(3\sigma_g^{-1}1\pi_g^2)$ state at $R = R_e$ goes to the second lowest dissociation limit and the second lowest $^2\Sigma_g^+(1\pi_u^{-1}1\pi_g3\sigma_u)$ state at $R = R_e$ goes to the lowest dissociation limit, if the configuration interaction was not included. In other words, this curve crossing is inevitable.

IV. IDENTIFICATION OF THE FORBIDDEN O_2^- COMPOUND STATES

In this section, we identify the forbidden O_2^- compound states, namely, the 8.5- and 13-eV compound states observed in the condensed phase, using Tables I and II.

A. O_2^- states arising from $3\sigma_u$, $1\pi_u^{-1}1\pi_g3\sigma_u$, and $3\sigma_g^{-1}1\pi_g3\sigma_u$

O_2^- states arising from the $3\sigma_u$, $1\pi_u^{-1}1\pi_g3\sigma_u$, and $3\sigma_g^{-1}1\pi_g3\sigma_u$ configurations autoionize by detaching the $3\sigma_u$ electron. Among these states, the $O_2^-(3\sigma_u)^4\Sigma_u^-$ state

has the largest electron attachment cross section [since it is an allowed one-electron excitation and has the higher multiplicity than the $O_2^-(3\sigma_u)^2\Sigma_u^-$ state]; the largest survival rate [since it has the smallest $\Delta W(R_e)$ and ΔR_{ec} parameters]; and the smallest width (see Table II). In other words, the $O_2^-(3\sigma_u)^4\Sigma_u^-$ state has the best conditions to be observed in the O^- yield curve. Therefore, if this state is not observed, the other states cannot be observed in the O^- yield curve.

The $O_2^-(3\sigma_u)^4\Sigma_u^-$ state dominates in the electron-impact vibrational excitation spectra over the 7–13 eV region, indicating a large electron attachment cross section. This state, however, does not appear in the O^- yield curve, indicating a negligibly small survival rate. Therefore, based on the argument given in the previous paragraph, we conclude that the other states arising from the $3\sigma_u$, $1\pi_u^{-1}1\pi_g3\sigma_u$, and $3\sigma_g^{-1}1\pi_g3\sigma_u$ configurations cannot be observed in the O^- yield curve. To sum up, all the states which autoionize by detaching the $3\sigma_u$ electron cannot yield O^- ions, because of their negligibly small survival rates.

The 8.5- and 13-eV compound states yield O^- ions in the condensed phase. For assigning these compound states, we can exclude the O_2^- states arising from the $3\sigma_u$, $1\pi_u^{-1}1\pi_g3\sigma_u$, and $3\sigma_g^{-1}1\pi_g3\sigma_u$ configurations, because they cannot yield O^- ions in both gas and solid phases and also have the W_{FC}'s which are too wide ($\gtrsim 4.3$ eV) for the observed linewidths ($\lesssim 2.2$ eV).

B. O_2^- states arising from $1\pi_g$, $1\pi_u^{-1}1\pi_g^2$, $3\sigma_g^{-1}1\pi_g^2$, and $2\sigma_u^{-1}1\pi_g^2$

To assign the 8.5- and 13-eV compound states, we can exclude the $O_2^-(1\pi_g)^2\Pi_g$ state since this state cannot produce O^- ions. It cannot produce O^- ions because its vertical energy (0.21 eV) is much lower than the lowest $O + O^-$ dissociation limit (3.65 eV). We can also exclude the $O_2^-(1\pi_u^{-1}1\pi_g^2)^2\Pi_u$ state, since this state yields ample O^- ions in the gas phase and has been assigned to the 7-eV feature. Consequently, for assigning the 8.5- and 13-eV compound states, we have only two O_2^- states left, the $^2\Sigma_g^+(3\sigma_g^{-1}1\pi_g^2)$ and $^2\Sigma_u^+(2\sigma_u^{-1}1\pi_g^2)$ states.

Comparing the vertical energies of these two states, we can assign them for the 8.5- and 13-eV compound states. This comparison can be done without calculations, because of the large binding-energy difference between the $2\sigma_u$ and $3\sigma_g$ electrons. We can certainly state that the vertical energy of the $^2\Sigma_u^+(2\sigma_u^{-1}1\pi_g^2)$ state is higher than that of the $^2\Sigma_g^+(3\sigma_g^{-1}1\pi_g^2)$ state. From this, we identify the $^2\Sigma_g^+(3\sigma_g^{-1}1\pi_g^2)$ and $^2\Sigma_u^+(2\sigma_u^{-1}1\pi_g^2)$ states as the 8.5- and 13-eV compound states, respectively. In the following section, we confirm these identifications.

C. Confirmation

Here, we show that the $^2\Sigma_g^+(3\sigma_g^{-1}1\pi_g^2)$ and $^2\Sigma_u^+(2\sigma_u^{-1}1\pi_g^2)$ states have appropriate characteristics of the 8.5- and 13-eV compound states.

(i) The survival rates of these two states are large enough to yield measurable O^- ions. We can state this based on the following argument: The survival rate of

the $^2\Pi_u(1\pi_u^{-1}1\pi_g^2)$ state must be large enough to yield O^- ions, since this state (i.e., the 7-eV compound state) dominates in the O^- yield curve. The two states have even larger survival rates than the $^2\Pi_u$ state, because these two states have smaller $\Delta W(R_e)$ and ΔR_{ec} parameters than the $^2\Pi_u$ state. Therefore, the survival rates of the two states must be large enough to yield O^- ions.

(ii) The observed resonance peak positions [8.5 (±0.5) and 13 (±1) eV] and their widths [2.2 (±0.3) and 2.1 (±0.4) eV] of the 8.5- and 13-eV peaks agree well with theoretical resonance peaks [8.0 (±0.9) and 14.2 (±0.9) eV] and their widths [2.3 (±0.4) and 2.1 (±0.4) eV] of the assigned states. The theoretical resonance peaks and widths are estimated from the vertical energies and the Franck-Condon widths listed in Table II, based on the argument presented in Appendix B.

(iii) The dissociation limits (1 and 2) of the 8.5- and 13-eV compound states agree with those (1 and 2) of the assigned states, respectively (compare Tables I and II).

(iv) The absence of the 8.5- and 13-eV peaks in the O^- yield from the O_2 gas are nicely explained by the forbidden electron attachment for the assigned states (see Table II).

Based on these confirmations, we conclude that the 8.5- and 13-eV peaks are due to the $^2\Sigma_g^+(3\sigma_g^{-1}1\pi_g^2)$ and $^2\Sigma_u^+(2\sigma_u^{-1}1\pi_g^2)$ resonance states. This identification implies that absence of these peaks in the gas phase is indeed due to the σ^- selection rule.

V. PREVIOUS INTERPRETATIONS

The 8.5- and 13-eV features have been interpreted previously. Xiang and Lichtman,[6] who reported the O^- yield curve from O_2/W (Fig. 1), attributed the 13-eV peak to the $O_2^-(1\pi_u^{-1}1\pi_g^2)^2\Pi_u$ state, or the "7-eV" state, which was regarded as shifted because of a substrate effect. They overlooked a weak 8.5-eV feature in their spectrum. Sanche and co-workers,[7,8] who reported the three O^- yield curves from O_2/Pt (Fig. 1) and the OH^--$C_6H_{14}/O_2/Pt$ spectrum in Fig. 2, assigned the $O_2^-(3\sigma_g^{-1}1\pi_g^2)^2\Sigma_g^+$ state (that is, the "8.5-eV" state) to the 13-eV feature. Further, the absence of the 13-eV feature in the gas-phase spectrum was attributed to the angular dependence rule given by Dunn,[2] rather than to the σ^- selection rule.[3] Mark et al.,[9] who reported the $O_2\cdot O^-$ and O_2^- yields from $(O_2)_n$ clusters (Fig. 2), attributed both the 7- and 8.5-eV features to the $O_2^-(1\pi_u^{-1}1\pi_g^2)^2\Pi_u$ state. Our analyses in this work do not support any of the above interpretations.

ACKNOWLEDGMENTS

APPENDIX A: VERTICAL ENERGIES

Here, we estimate the vertical energies of O_2^- states using semiempirical methods.

Tables IV, V, and VI list the observed and estimated vertical energies measured from the O_2 ground state to the O_2, O_2^+, and O_2^- valence states, respectively. The valence states are identified by their electronic configurations and state symmetries except for the three $O_2^+(1\pi_u^{-1})^2\Pi_u$ states, which have additional labels, I, II, or III. When a valence state mixes strongly with Rydberg states, such as the O_2 $^3\Pi_u(1\pi_u^{-1}3\sigma_u)$ valence state

TABLE IV. Observed and estimated vertical energies (eV) of the lower-lying O_2 states. Estimated energies are enclosed in parentheses.

Electronic configuration	Configuration center (eV)	State symmetry	Vertical energy (eV)	Reference
Ground state	0.60	$^3\Sigma_g^-$	0.00	23
		$^1\Delta_g$	0.98	23
		$^1\Sigma_g^+$	1.63	23
$1\pi_u^{-1}1\pi_g$	7.5	$^1\Sigma_u^-$	5.8	23,24
		$^3\Delta_u$	6.0	23,24
		$^3\Sigma_u^+$	6.1	23,24
		$^3\Sigma_u^-$	8.5	24
		$^1\Delta_u$	(10.8)	25
		$^1\Sigma_u^+$	(12.6)	25
$3\sigma_g^{-1}1\pi_g$	8.1	$^3\Pi_g$	7.7	26
		$^1\Pi_g$	(9.2)	25
$1\pi_g^{-1}3\sigma_u$	10.6	$^3\Pi_u$	10.2	27
		$^1\Pi_u$	(11.9)	25
$2\sigma_u^{-1}1\pi_g$	14.3	$^3\Pi_u$	14.2	28
		$^1\Pi_u$	(14.6)	25
$2\sigma_g^{-1}1\pi_g$	28.9 ± 1.0	$^3\Pi_g$	28.5 ± 1.0	29
		$^1\Pi_g$	$(30.0)^a$	

^{a}Estimated from the splitting energies of the $3\sigma_g^{-1}1\pi_g$ states.

TABLE V. Observed and estimated vertical energies (eV) of the lower-lying O_2^+ states. Estimated energies are enclosed in parentheses.

Electronic configuration	Configuration center (eV)	State symmetry	Vertical energy (eV)	Reference
$1\pi_g^{-1}$	12.31	$^2\Pi_g$	12.31	30
$1\pi_u^{-1}$	19.2	$^4\Pi_u$	16.70	30
		$^2\Pi_u(I)$	17.73	30
		$^2\Phi_u$	19.1	31
		$^2\Pi_u(II)$	(20.8)	32
		$^2\Pi_u(III)$	24.0	30
$3\sigma_g^{-1}$	19.6	$^4\Sigma_g^-$	18.17	30
		$^2\Delta_g$	19.90	31
		$^2\Sigma_g^-$	20.43	30
		$^2\Sigma_g^+$	(20.8)	31
$2\sigma_u^{-1}$	25.9	$^4\Sigma_u^-$	24.58	30
		$^2\Delta_u$	(26.0)	31
		$^2\Sigma_u^+$	(26.8)	31
		$^2\Sigma_u^-$	27.3	33
$2\sigma_g^{-1}$	40.0	$^4\Sigma_g^-$	38.8	34[a]
		$^2\Delta_g$	(40.3)[b]	
		$^2\Sigma_g^-$	40.8	34[a]
		$^2\Sigma_g^+$	(41.1)[b]	

[a]The energy scale is shifted by 0.8 eV to make the first-peak energy position agree with the accurate energy 12.3 eV.
[b]Estimated from the splitting energies of the $3\sigma_g^{-1}$ states.

with the $^3\Pi_u(1\pi_g^{-1}3p\sigma_u)$ Rydberg state, the pure valence state energy is estimated from analyses presented in the literature. All the vertical energies listed in the three tables represent pure valence state energies. The references on which the experimental data or analyses are based are cited in the tables. In these three tables, estimated (as opposed to observed) vertical energies are enclosed in parentheses.

With the unobserved $O_2^+(1\pi_u^{-1})^2\Pi_u(II)$ state, we exemplify an empirical method used to estimate a vertical energy. First, we estimate the vertical energy difference for $O_2^+(1\pi_u^{-1})^2\Pi_u(II)$-$O_2^+(1\pi_u^{-1})^4\Pi_u$ and then the vert-

TABLE VI. Observed and estimated vertical energies (eV) of the lower-lying O_2^- states. Estimated energies are enclosed in parentheses.

Electronic configuration	Configuration center (eV)	State symmetry	Vertical energy (eV)	Reference
$1\pi_g$	0.21	$^2\Pi_g$	0.21	35
$1\pi_u^{-1}1\pi_g^2$	7.8±0.2	$^2\Pi_u$	7.8±0.2	18[a]
$3\sigma_u$	10.6±0.3	$^4\Sigma_u^-$	9.5±0.3	36
		$^2\Delta_u$	(10.7)[b]	
		$^2\Sigma_u^+$	(11.5)[b]	
		$^2\Sigma_u^-$	(11.9)	19[c]

[a]The uncertainty indicates the sensitivity of the fitting and thus does not reflect absolute errors.
[b]Estimated from the splitting energies of the $2\sigma_u^{-1}$ states.
[c]Estimated using the $^4\Sigma_u^- - {}^2\Sigma_u^-$ energy difference calculated by MCSCF with 65 configurations.

ical energy of the $O_2^+(1\pi_u^{-1})^2\Pi_u(II)$ state. In Table VII, relative vertical energies of states arising from the electron configuration $O_2^+(1\pi_u^{-1})$ are listed, where the relative energies are measured from the lowest state $O_2^+(1\pi_u^{-1})^4\Pi_u$. In the table, "experiment" and "theory" columns list the observed and calculated relative vertical energies. Note that the experimental energy for the $O_2^+(1\pi_u^{-1})^2\Pi_u(II)$ state is missing and to be estimated. The ratios between experimental and theoretical values, which are listed in the last column, are almost constant. Our empirical estimate is based on this constancy. Assuming the missing ratio for the $^2\Pi_u(II)$ state to be 1.2, we estimate the relative energy for this state to be 4.1 eV ($=3.4\times1.2$). In other words, the vertical energy difference $O_2^+(1\pi_u^{-1})^2\Pi_u(II)$-$O_2^+(1\pi_u^{-1})^4\Pi_u$ is estimated to be 4.1 eV. With this and the observed vertical energy 16.70 eV for the $O_2^+(1\pi_u^{-1})^4\Pi_u$ state, the $O_2^+(1\pi_u^{-1})^2\Pi_u(II)$ state energy is estimated to be 20.8 eV ($=16.7+4.1$). This estimated energy is listed in Table V and enclosed in parentheses. The theoretical calculations utilized are cited in the "reference" columns. When theoretical calculations are not available, such as for the $2\sigma_g^{-1}$ and $2\sigma_g^{-1}1\pi_g$ cases, we use the relative energies of analogous EC's, such as $3\sigma_g^{-1}$ and $3\sigma_g^{-1}1\pi_g$, for the above cases.

The configuration center (CC) of an electronic configuration (EC) is defined as a weighted average of state energies arising from the EC. Tables IV, V, and VI include such CC's, which are calculated from the vertical energies. The averaged vertical excitation energy (AVEE) can be calculated from a pair of CC's. For example, the AVEE for the $1\pi_u \rightarrow 1\pi_g$ excitation can be calculated from the differences of the following three pairs: $O_2^+1\pi_u^{-1}$ and $1\pi_g^{-1}$, $O_2 1\pi_u^{-1}1\pi_g$, and the ground-state configuration of O_2, or $O_2^- 1\pi_v^{-1}1\pi_g^2$ and $1\pi_g$. Table VIII compares the AVEE's calculated from the different pairs of CC's. This comparison clearly shows that the AVEE's are nearly independent of the molecular charge. Assuming the charge independence, we can often predict the CC's of O_2^- states with an uncertainty of less than 1 eV.

There are several ways to estimate the unobserved vertical energies of the O_2^- compound states. For example, we can estimate the vertical CC of the $3\sigma_g^{-1}1\pi_g^2$ configuration from any of the following three equations:

TABLE VII. Relative vertical energies (eV) of states arising from the electronic configuration $O_2^+(1\pi_u^{-1})$. The relative energies are measured from the lowest state $O_2^+(1\pi_u^{-1})^4\Pi_u$. Ratio is given by experiment and theory.

State	Experiment	Theory[a]	Ratio
$^4\Pi_u$	0.0	0.0	
$^2\Pi_u(I)$	1.0	0.9	1.1
$^2\Phi_u$	2.4	2.0	1.2
$^2\Pi_u(II)$		3.4	
$^2\Pi_u(III)$	7.3	6.1	1.2

[a]Reference 32.

$$3\sigma_g^{-1}1\pi_g^2 - 1\pi_g(0.2 \text{ eV}) = 7.5 \text{ eV} , \qquad (A1)$$

$$3\sigma_g^{-1}1\pi_g^2 - 1\pi_u^{-1}1\pi_g^2 \ (7.8 \text{ eV}) = 0.6 \text{ eV} , \qquad (A2)$$

$$3\sigma_g^{-1}1\pi_g^2 - 3\sigma_u(10.6 \text{ eV}) = -2.5 \text{ eV} , \qquad (A3)$$

where the right-hand sides of the above equations are the AVEE's for O_2 listed in Table VIII. Although we could use the AVEE's for O_2^+ instead of O_2, we prefer the O_2 data to the O_2^+ data because the total charge difference between O_2 and O_2^- is smaller than that between O_2^+ and O_2^-. These equations give the $3\sigma_g^{-1}1\pi_g^2$ energy as 7.7, 8.4, and 8.1 eV, respectively. Averaging these three, we estimate the $3\sigma_g^{-1}1\pi_g^2$ energy to be 8.1 eV with a probable uncertainty of ± 0.9 eV. This and similarly estimated vertical energies for the lower-lying O_2^- valence states are listed in Table II.

APPENDIX B: ESTIMATION OF RESONANCE-PEAK POSITION AND ITS WIDTH FROM VERTICAL ENERGY AND FRANCK-CONDON WIDTH

Vertical energy and Franck-Condon width may not agree with a resonance peak and its width observed in the O^- yield curve because of autoionization. Figure 7 schematically shows how autoionization induces this disagreement. In the figure, the $W^-(R)$ and $W(R)$ denotes, as in Fig. 5, the potential-energy curves of the O_2^- and O_2 states, where the O_2^- state autoionizes into the O_2 state. The electron attachment cross section, $\sigma_{AT}(E)$, has a peak at a vertical energy because of the Franck-Condon principle and its width gives the Franck-Condon width. On the other hand, a resonance peak and its width in the O^- yield curve are given by a peak and its width of the dissociative attachment cross section $\sigma_{DA}(E)$. According to Eq. (10), the $\sigma_{AT}(E)$ and $\sigma_{DA}(E)$ is related by $\sigma_{DA}(E) = \sigma_{AT}(E)SF(E)$, where $SF(E)$ denotes the exponential factor in Eq. (10) and represents the probability that the O_2^- state survives against the autoionization. Because of this $SF(E)$ factor, resonance peaks and widths of $\sigma_{DA}(E)$ and $\sigma_{AT}(E)$ may not agree with each other.

The functional form of $SF(E)$ can be deduced from the expression given in Eq. (10). Namely, the $SF(E)$ is unity
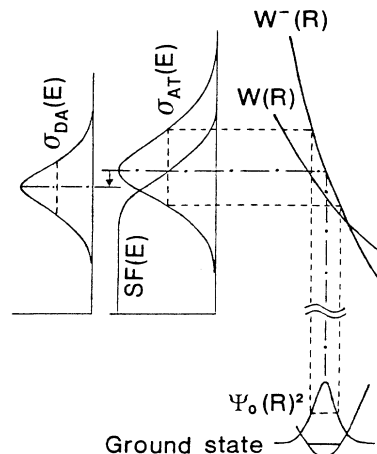
FIG. 7. Schematic diagram illustrating the two effects: the shift of the $\sigma_{DA}(E)$ peak position relative to the $\sigma_{AT}(E)$ peak and the smaller $\sigma_{DA}(E)$ width in comparison with the $\sigma_{AT}(E)$ width.

below the $E = W^-(R_C)$ and decreases monotonously with increasing E, where R_C denotes the crossing point of the $W^-(R)$ and $W(R)$ curves. [This is because $\Gamma = 0$ below the $E = W^-(R_C)$; the integrand $\Gamma(R)/\hbar V(R)$ is always positive; and the lower integration limit (R_E) decreases with increasing E.] From this functional form of the $SF(E)$, we can conclude that a peak position of the $\sigma_{DA}(E)$ is lower than that of the $\sigma_{AT}(E)$, and its width of the $\sigma_{DA}(E)$ is narrower than that of the $\sigma_{AT}(E)$. Furthermore, we can state that the larger the $\Delta W(R_e)$ and ΔR_{ec} parameters, the larger the lowering of peak position and the narrowing of width.

For the $O_2^-(1\pi_u^{-1}1\pi_g^2)^2\Pi_u$ resonance state, the observed peak position (6.7 eV) in the O^- yield curve is lower than the vertical energy (7.8 eV), and the observed line width (2.0 eV) in the O^- yield curve is narrower than the Franck-Condon width (3.0 eV),[18] agreeing with the above predictions. Because the $\Delta W(R_e)$ and ΔR_{ec} parameters of this resonance state is large, the shift (1.1 eV) in the peak position and the reduction (1.0 eV) in the

TABLE VIII. Comparison of averaged vertical excitation energies (eV). GSC represents the ground-state configuration.

Excitation	O_2^+	O_2	O_2^-
$1\pi_u \rightarrow 1\pi_g$	6.9	6.9	7.6 ± 0.2
	$(1\pi_u^{-1} - 1\pi_g^{-1})$	$(1\pi_u^{-1}1\pi_g - \text{GSC})$	$(1\pi_u^{-1}1\pi_g^2 - 1\pi_g)$
$3\sigma_g \rightarrow 1\pi_g$	7.3	7.5	
	$(3\sigma_g^{-1} - 1\pi_g^{-1})$	$(3\sigma_g^{-1}1\pi_g - \text{GSC})$	
$1\pi_g \rightarrow 3\sigma_u$		10.0	10.4 ± 0.3
		$(1\pi_g^{-1}3\sigma_u - \text{GSC})$	$(3\sigma_u - 1\pi_g)$
$2\sigma_u \rightarrow 1\pi_g$	13.6	13.7	
	$(2\sigma_u^{-1} - 1\pi_g^{-1})$	$(2\sigma_u^{-1}1\pi_g - \text{GSC})$	
$2\sigma_g \rightarrow 1\pi_g$	27.7	28	
	$(2\sigma_g^{-1} - 1\pi_g^{-1})$	$(2\sigma_g^{-1}1\pi_g - \text{GSC})$	

width are large. The $O_2^-(3\sigma_g^{-1}1\pi_g^2)^2\Sigma_g^+$ and $O_2^-(2\sigma_u^{-1}1\pi_g^2)^2\Sigma_u^+$ states have much smaller $\Delta W(R_e)$ and ΔR_{ec} parameters than the $^2\Pi_u$ resonance state (see Table II). Therefore, we expect the smaller shift (0.1 eV)

and reduction (0.1 eV) for these two states in comparison with those for the $^2\Pi_u$ resonance state. Using these small shift and reduction, we estimated the theoretical resonance peak positions and widths.

[1] D. C. Cartwright, S. Trajmar, W. Williams, and D. L. Huestis, Phys. Rev. Lett. **27**, 704 (1971).

[2] G. H. Dunn, Phys. Rev. Lett. **8**, 62 (1962).

[3] H. Sambe and D. E. Ramaker, Chem. Phys. Lett. **139**, 386 (1987).

[4] A. M. Bass and H. P. Broida, J. Mol. Spectrosc. **12**, 221 (1964).

[5] D. Rapp and D. D. Briglia, J. Chem. Phys. **43**, 1480 (1965).

[6] L. Z. Xiang and D. Lichtman, Surf. Sci. **114**, 287 (1982).

[7] R.Azria, L. Parenteau, and L. Sanche, Phys. Rev. Lett. **59**, 638 (1987).

[8] L. Sanche and L. Parenteau, Phys. Rev. Lett. **59**, 136 (1987).

[9] T. D. Märk, K. Leiter, W. Ritter, and A. Stamatovic, Phys. Rev. Lett. **55**, 2559 (1985).

[10] R. Azria, L. Parenteau, and L. Sanche, J. Chem. Phys. **87**, 2292 (1987).

[11] G. J. Schulz, Rev. Mod. Phys. **45**, 423 (1973).

[12] L. Sanche and M. Michaud (unpublished).

[13] J. N. Bardsley, A. Herzenberg, and F. Mandl, Proc. Phys. Soc. London **89**, 321 (1966).

[14] D. T. Birtwistle and A. Herzenberg, J. Phys. B **4**, 53 (1971); J. M. Blatt and V. F. Weisskopf, *Theoretical Nuclear Physics* (Wiley, New York, 1952), p. 390, Eq. (7.15).

[15] J. G. Winans and E. C. G. Stueckelberg, Proc. Nat. Acad. Sci. U.S.A. **14**, 867 (1928).

[16] G. Herzberg, *Molecular Spectra and Molecular Structure* (Van Nostrand, New York, 1950), Vol. 1.

[17] A. S. Coolidge, H. M. James, and R. D. Present, J. Chem. Phys. **4**, 193 (1936).

[18] T. F. O'Malley, Phys. Rev. **155**, 59 (1967).

[19] G. Das, A. C. Wahl, W. T. Zemke, and W. C. Stwalley, J. Chem. Phys. **68**, 4252 (1978).

[20] E. Wigner and E. E. Witmer, Z. Phys. **51**, 859 (1928).

[21] M. Krauss et al., Phys. Rev. A **7**, 69 (1973).

[22] H. H. Michels and F. E. Harris, in *Proceedings of the Seventh International Conference on the Physics of Electronic and Atomic Collisions, Amsterdam, 1971*, edited by T. Govers and F. J. de Heer (North-Holland, Amsterdam, 1971), Vol. II, p. 1170.

[23] K. P. Huber and G. Herzberg, *Molecular Spectra and Molecular Structure—Constants of Diatomic Molecules* (Van Nostrand Reinhold, New York, 1979).

[24] K. Wakiya, J. Phys. B **11**, 3931 (1978).

[25] R. P. Saxon and B. Liu, J. Chem. Phys. **67**, 5432 (1977).

[26] D. Spence, J. Chem. Phys. **74**, 3898 (1981).

[27] R. J. Buenker, S. D. Peyerimhoff, and M. Peric, Chem. Phys. Lett. **42**, 383 (1976); L. C. Lee, T. G. Slanger, G. Black, and R. L. Sharpless, J. Chem. Phys. **67**, 5602 (1977).

[28] H.-J. Hinz, in *Proceedings of the 4th International Conference on Vacuum Ultraviolet Radiation Physics, Hamburg, 1974*, edited by E. E. Koch (Pergamon, Oxford, 1974), p. 176.

[29] J. S. Lee, J. Chem. Phys. **67**, 3998 (1977).

[30] O. Edqvist, E. Lindholm, L. E. Selin, and L. Åsbrink, Phys. Scripta. **1**, 25 (1970).

[31] N. Jonathan et al., J. Chem. Soc. Faraday Trans. II **70**, 1810 (1974).

[32] R. N. Dixon and S. E. Hull, Chem. Phys. Lett. **3**, 367 (1969).

[33] M. S. Banna and D. A. Shirley, J. Electron Sepctrosc. Relat. Phenom. **8**, 255 (1976).

[34] K. Siegbahn et al., *ESCA Applied to Free Molecules* (North-Holland, Amsterdam, 1969).

[35] R. J. Celotta et al., Phys. Rev. A **6**, 631 (1972).

[36] S. F. Wong, M. J. W. Boness, and G. J. Schulz, Phys. Rev. Lett. **31**, 969 (1973).